ARTICLES

In situ Observation of Nucleation and Crystal Growth in Zeolite Synthesis. A Small-Angle X-ray Scattering Investigation on Si-TPA-MFI

Peter-Paul E. A. de Moor,* Theo P. M. Beelen, and Rutger A. van Santen

Schuit Institute of Catalysis, Eindhoven University of Technology, P.O. Box 513, 5600 MB Eindhoven, The Netherlands

Received: June 9, 1998

The formation and consumption of nanometer scale precursor particles during the hydrothermal synthesis of Si-TPA-MFI from a clear solution has been studied *in situ* using a combination of X-ray scattering techniques and with electron microscpy. The combination of wide-, small-, and ultra-small-angle X-ray scattering allowed us to obtain information on a continuous range of length scales spanning over four orders of magnitude (0.17−6000 nm), covering all particle populations present during the complete course of the crystallization process. The use of high-brilliance synchrotron radiation allows us to perform time-resolved experiments. Two types of precursor particles were observed: 2.8 nm sized primary units and aggregates (≈10 nm). Variation of the alkalinity of the synthesis mixture revealed a strong correlation between the concentration of the aggregates and the rate of the crystal nucleation. The presence of the 2.8 nm sized primary units appears to be independent on the alkalinity. The addition of seed crystals to a synthesis mixture that does not show spontaneous nucleation (no aggregates observed) resulted in normal crystal growth. The size distribution of the growing crystals could be followed *in situ* by fitting calculated scattering patterns to experimental curves and showed good agreement with electron microscopy results. The apparent activation energy for crystal growth is determined to be 83 kJ/mol by following *in situ* the crystal growth process at various reaction temperatures. These data show that the formation of aggregates of primary units is an essential step in the nucleation process and suggest that the crystal growth step is the reaction-controlled inclusion of the 2.8 nm sized primary units at the crystal surface.

Introduction

Zeolites are crystalline, microporous, aluminosilicates which are used in a broad variety of applications as molecular sieves (e.g. separation processes), as catalysts (e.g. as cracking catalysts in petrol refining), and as ion-exchange agent.[1] Improvement of known applications and the prospect of new ones are a continuing driving force to investigate the possibility to synthesize zeolites with new (combinations) of properties.[2] Therefore, there is significant research to understand the mechanism of the assembly of small entities to zeolites with the ultimate goal of being able to create zeolites by rational design.[3]

The vast majority of zeolites are synthesized under hydrothermal conditions from alkaline aqueous solutions. Traditionally, investigations of zeolite synthesis were mainly based on observations on end products in relation with changes of the reactants and the process conditions. Recently, using NMR spectroscopy, information was obtained on the structure of the silicate species in the synthesis mixture (for example see ref 4), and on the interactions between silicate species and the organic structure directing agents.[5,6] In general, these spectroscopic methods showed the importance of effective interaction of the organic molecules with the silicate species, but did not give information on the nanometer structure of the entities in solution. Therefore, there is an information gap between the molecular scale entities present in solution and the crystal structures formed. The main reason for this gap is the fundamental problem that most spectroscopic methods do not allow to probe structures which are much larger than molecules (typically larger than 1 nm). Furthermore, one prefers to perform *in situ* experiments since the intermediates in solution are expected to be build by relatively weak bonds and strongly depending on the surrounding solution, and therefore drying will most likely be destructive.

The above problems can be circumvented using scattering of X-rays at (very) small angles. With high-brilliance synchrotron radiation, we are also able to perform time-resolved experiments. By simultaneously measuring the scattering at small and wide angles (respectively SAXS and WAXS), correlations could be found between the (trans)formations of nanometer scale structures and the presence of crystalline structures. Using ultra-small-angle scattering (USAXS), we are able to probe the scattering at the surface of the crystals.[7] From these data we can follow *in situ* the evolution of the particle size distribution of the product crystals.

Using these techniques, we investigated the crystallization of Si-TPA-MFI during the complete course of the reaction. The

* Author of correspondence. Fax: +31 40 2455054. E-mail: ppaul@sg3.chem.tue.nl.

10.1021/jp982553q CCC: $18.00
Published on Web 02/20/1999

presence of two types of nanometer scale precursors could be demonstrated: 2.8 nm primary units and aggregates (≈10 nm) composed of these units. The alkalinity of the synthesis mixture has been varied and appears to have an influence on both the formation of the aggregates and the crystallization behavior. Combined with crystallizations with seed crystals added, these results show the importance of the aggregation of the primary units in the nucleation process. The temperature dependence of the growth of the crystals revealed that this is a reaction-controlled process, which probably involves the integration of primary units at the growing crystal.

Experimental Section

Syntheses. Si-TPA-MFI synthesis mixtures with composition 10.0 SiO_2:2.44 TPAOH:*x*NaOH:114 H_2O were prepared according to a recipe based on a Exxon Chemical patent.[8] The alkalinity, expressed as the ratio Si/OH in the synthesis mixture, was varied by changing the amount of NaOH. Si/OH ratios of 2.12, 2.42, 2.57, 2.72, and 3.02 correspond with $x = 2.28$, 1.70, 1.45, 1.24, and 0.87, respectively. The preparation method will be outlined here for a synthesis mixture having Si/OH = 3.02.

1.40 g of NaOH (Merck, p.a.) was dissolved in 100 g of tetrapropylammonium hydroxide (Merck, 20 wt % TPAOH in H2O) with gentle mixing at room temperature, followed by spoonwise addition of 27.0 g of silicic acid powder (Baker, 10.2 wt % H_2O). Thereafter, the homogeneous disperson was boiled under stirring for approximately 10 min to obtain a clear solution. The solution was cooled down to room temperature in a water bath, corrected for loss of water during boiling, and filtered through a paper filter (Schleicher & Schüll, Schwarzband), and successively through a 0.45 μm filter (Schleicher & Schüll, Spartan 30/B). The reaction mixtures were completely clear and aged for less than 1 h at room temperature before heating to a reaction temperature of 125 °C. All scattering measurements were performed *in situ* in a special rotating (2 rpm), electrically heated sample cell. The sample thickness was 0.5 mm and mica windows (thickness 0.25 μm) were used.

Seeds. The Si-TPA-MFI seed crystals were prepared from a synthesis mixture having Si/OH = 3.02 which was heated for 18 h. at 95 °C. The seeds were separated from the mother liquor by centrifugation and decantation, after which they were redispersed in deionised water using an ultrasonic bath. This washing treatment was repeated three times and resulted in a stable colloidal crystal dispersion. The seeds were added to the synthesis mixture just before heating to reaction temperature. The amount of SiO_2 added by the crystals was calculated on basis of the amount of SiO_2 in the synthesis mixture.

The number of crystals in the product compared to the number of seeds added to the fresh synthesis mixture can be can be expressed as the fraction f_s:

$$f_s = \frac{N_{crystal}}{N_{seed}} = \frac{\bar{V}_{seed}}{\bar{V}_{crystal}}\left(1 + \frac{x}{p}\right) \quad (1)$$

Here N_{part} refers to the number of particles, x is the fraction SiO_2 converted to MFI, and p is the weight fraction of seeds added. $\bar{V}_{part}$ is the average volume of the particle population. The subscript seed refers to the seed crystals, whereas the subscript crystal refers to the crystals in the final product.

SAXS and Bonse-Hart Setup. The combined SAXS and WAXS experiments were performed at station 8.2 of the Synchrotron Radiation Source at Daresbury Laboratory (United Kingdom),[9] using a camera length of 0.8 ($0.4 < Q < 7$ nm^{-1}) and 3.4 m ($0.1 < Q < 2.5$ nm^{-1}). Using high-intensity synchrotron radiation and position-sensitive detectors, we were able to collect a SAXS and WAXS pattern simultaneously with a good signal to noise ratio every 2 min. The data was normalized for the intensity of the X-ray beam and corrected for detector sensitivity prior to background correction. The scattering from water at reaction temperature was used as background pattern. For the calibration of the SAXS and WAXS patterns, respectively, the scattering of an oriented specimen of wet rat tail collagen and the diffraction of a fully crystallized sample of zeolite NaA were used. The wavelength for station 8.2 is fixed at 1.54 Å.

The USAXS experiments have been performed at the high-brilliance beamline ID2/BL4 of the European Synchrotron Radiation Facility in Grenoble (FR) using a Bonse-Hart type of camera[10] ($0.001 < Q < 0.3$ nm^{-1}). A configuration with two analyzer crystals was used, so no desmearing was necessary. The first analyzer crystal (Si(220)) was used to scan the angle, and there were three reflections in the horizontal plane. A second analyzer crystal (Si(111), two reflections) was used as a collimator in the vertical direction in order to obtain a comparable angular resolution in both vertical and horizontal directions. The wavelength of the X-rays was 0.1 Å. A NaI scintillator was used as detector, which shows a linear response over 4 decades of intensity. Several scans (4−5) over different 2Θ ranges with sufficient overlap were recorded using different degrees of attenuation of the incident X-ray beam, in order to have intensities on the detector in the linear range. Because of the high brilliance of the undulator beamline ID2, a complete pattern could be recorded in only 15 min despite the inherent low efficiency of the Bonse-Hart setup and the scanning mode of recording.

The Q ranges obtained with the USAXS, SAXS, and WAXS showed sufficient overlap to allow an accurate merging of the patterns.

SAXS Data Analysis. SAXS data provide information about the presence of different particle populations and some of their properties like particle size distribution, their shape, and the type of their interactions. The size distribution of the (growing) crystals in the synthesis mixtures was determined by fitting the calculated scattering pattern of a population of interacting spheres to the measured curve. In the calculation of the form factor, the crystals were assumed to have a normal size distribution and a spherical shape.[7,11] For calculating the structure factor, the Percus-Yevick approximation for hard-sphere interactions was applied. The influence of the polydispersity on the structure factor was taken into account using the "local monodisperse approximation" of Pedersen,[12] which gives good results up to volume fractions of 0.4. In our experiments, the volume fraction of crystals in the mother liquor will be typically 0.05 at full crystallization. The small contribution of the structure factor to the calculated intensity was included for completion.

The basic data correction, the analysis of the time-resolved data, and the interactive fitting of a calculated scattering pattern to measured data were performed using an in-house developed GUI-based program called Analyze, written in the IDL programming language.

Electron Microscopy. The samples for the transmission electron microscopy (EM) experiments were prepared in the synthesis cell used for the SAXS/WAXS and USAXS experiments under the same conditions. After rapid cooling of the cell to room temperature at a chosen reaction time, the sample was filtered and washed extensively with deionized water over a 0.02 μm filter (Whatman, Anodisk).

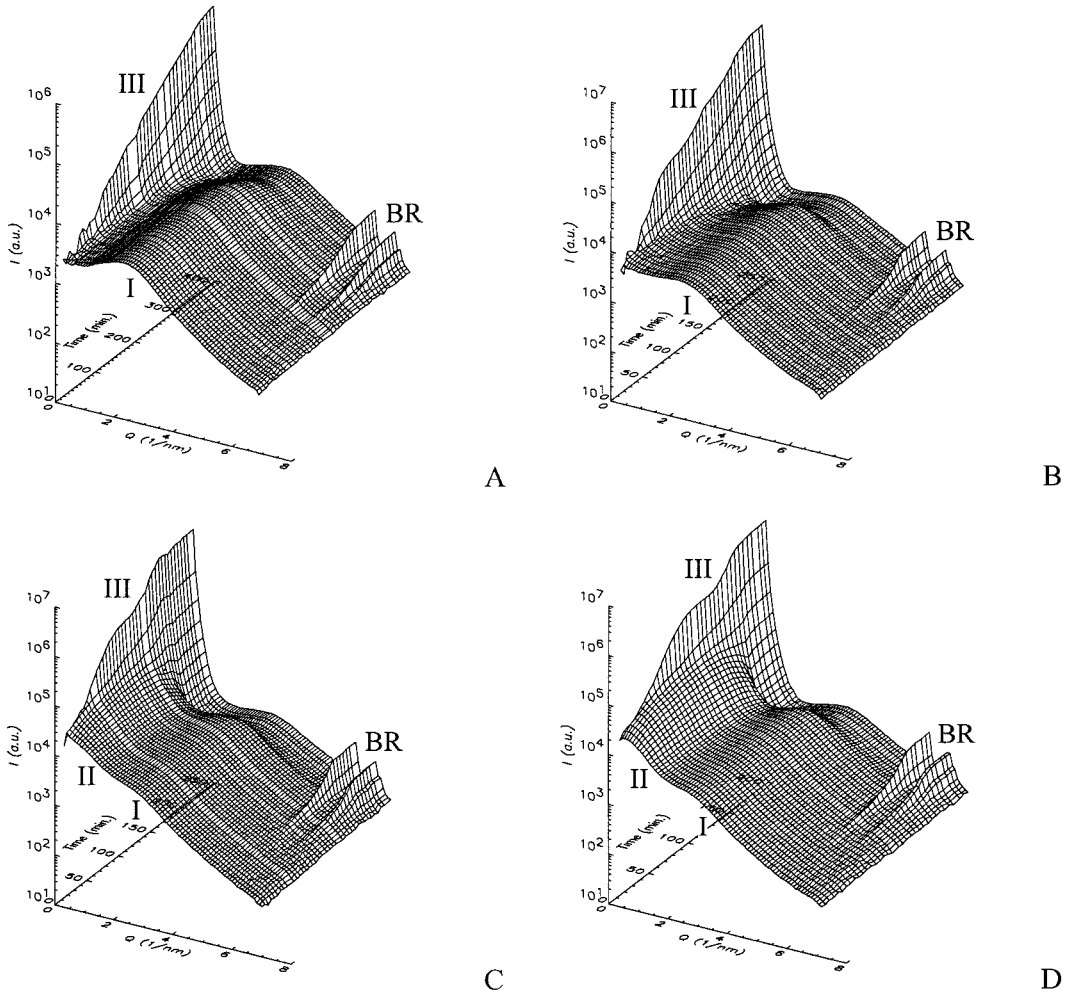

Figure 1. Time-resolved SAXS patterns for Si-TPA-MFI synthesis for different Si/OH ratios: (A) 2.42, (B) 2.57, (C) 2.72, (D) 3.02. Scattering particle types: I = primary units, II = aggregates, III = crystals, BR = Bragg reflections.

Transmission electron microscopy was performed at Delft university using a Philips CM 30 T electron microscope with an LaB_6 filament as the source of electrons operated at 300 kV. Samples were mounted on a carbon polymer supported on a copper grid by rubbing the grid against the filter containing the sample, followed by sputtering with carbon to decrease charging in the microscope.

Results

SAXS and WAXS Patterns during Si-TPA-MFI Syntheses at Different Alkalinities. The crystallization of Si-TPA-MFI at 125 °C from completely water clear synthesis mixtures with varying alkalinity (expressed in the ratio Si/OH) was studied *in situ* with simultaneous SAXS and WAXS. The time-resolved scattering patterns are depicted in Figure 1. The upper limit of the plotted Q range (d spacing ≈0.9 nm) is chosen to reveal the formation of the first Bragg reflections. The lower Q limit (d spacing ≈50 nm) is determined by the smallest angle which can be probed at station 8.2 at Daresbury Laboratory. Independent of the alkalinity, a broad hump is observed around $Q \approx 2$ nm^{-1} which intensity decreases during the crystallization (as observed by the growth of the Bragg reflections in the high Q region). This hump is due to scattering at a particle population which we will refer to as the primary units, with an estimated average size of 2.8 nm ($d_{part} = 2\pi/Q_{max}$). At very low Q values (large d spacings), an increasing scattering intensity is observed for every alkalinity, corresponding with scattering at large structures. This increasing intensity is due to the scattering at the surface of the growing crystals (confirmed by USAXS, ref 7). Between the hump at $Q \approx 2.2$ nm^{-1} and the scattering at the crystals at very low Q values, an alkalinity-dependent shoulder is observed, which is most apparent for the synthesis mixture with Si/OH = 3.02 (Figure 1D). The size of particles giving rise to the increased intensity is approximately 10 nm, and they are believed to be aggregates of the 2.8 nm sized primary units. The formation of these aggregates is more pronounced when the alkalinity decreases (in the order A, B, C, D in Figure 1). As the crystallization starts, the scattered intensity at the aggregates decreases.

Details of the scattering curves and the changes therein are more clear in Figure 2, showing snapshots at various reaction times. For each alkalinity, the following curves have been plotted (note the increasing reaction times at increasing alkalinity): (1) after 10 min of heating; (2) at the onset of crystallization as determined by the appearance of the first sign of Bragg reflections; (3) when the area of the Bragg reflections is approximately 50% of their final value; and (4) when the area of the Bragg reflections reached its final value.

These curves show the presence of the hump around $Q \approx 2.2$ nm^{-1} due to the scattering at the primary particles as well as the increasing intensity at very low Q values from the scattering at the crystals formed. Now the effect of the alkalinity on the formation of aggregates of primary units is clearly seen at $Q \approx 1$ nm^{-1}. For relatively high alkalinity (Si/OH = 2.42,

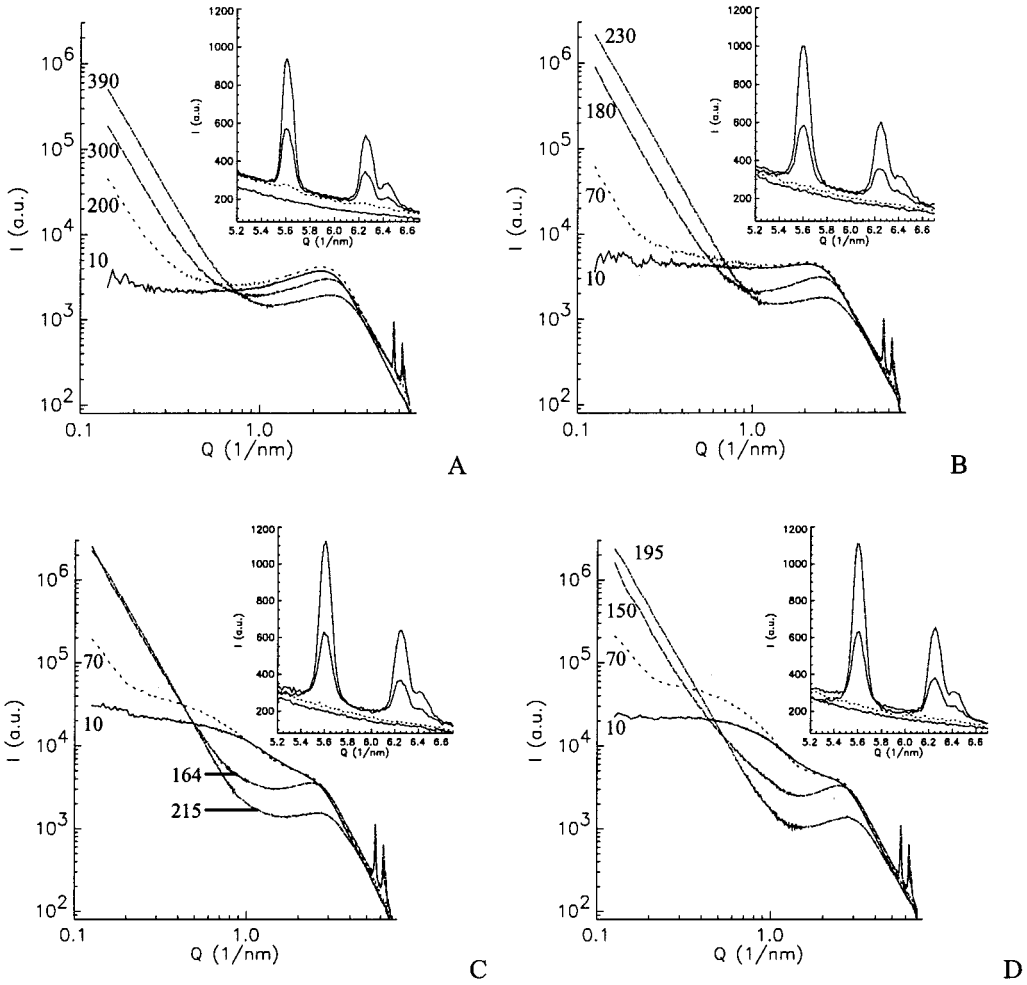

Figure 2. SAXS patterns after various reaction times for Si-TPA-MFI synthesis mixtures with different Si/OH ratios: (A) 2.42, (B) 2.57, (C) 2.72, (D) 3.02. The curves correspond to the following stages in the crystallization process (reaction times annotated at curves in min.): (1) shortly after heating, (2) onset of crystallization, (3) ≈50% crystallization, (4) full crystallization. The inset of each plot shows a close-up on the Bragg reflections in the high-*Q* region.

Figure 2A), the formation of aggregates is not clearly observed. If the alkalinity increases, the presence of a shoulder around $Q \approx 1$ nm^{-1} is more pronounced. The scattering patterns from the synthesis mixtures with Si/OH = 2.72 and 3.02 show the size of the aggregates to increase between 10 and 70 min of heating. For all alkalinities we observed a decrease in scattering intensity at the primary units and their aggregates (if present) between the onset of crystallization (second curve in Figure 2, A−D) and full crystallization (fourth curve). However, the consumption of both precursor particle types appears not to start at the same time: for the synthesis mixtures with the lowest alkalinities, a decrease in scattering intensity from the ≈10 nm aggregates (Figure 2, C and D, going from second to third curve) is clearly observed before the decrease in intensity due to the 2.8 nm primary units (going from third to fourth curve).

In order to obtain more information about the correlation between the presence of the different particle populations, the evolution of the scattering intensity at fixed angles has been plotted together with the area of the Bragg reflections as a measure of the conversion of the silica to the product Si-TPA-MFI crystals (Figure 3). For synthesis mixtures where the formation of ≈10 nm sized aggregates is observed (Si/OH = 2.57, 2.72, and 3.02, Figure 3B,C,D), the time of the osnet of crystallization as determined from the appearance of the Bragg reflections in the WAXS (verticle dotted lines) coincides with the maximum in scattered intensity from the aggregates. The decrease in intensity at a *d* spacing of 2.8 nm (primary units) starts significantly later. Only for the high-alkalinity synthesis mixture (Si/OH = 2.42) does the onset of crystallization coincide with the start of the decrease of scattering intensity at the 2.8 nm particles.

To show the influence of the alkalinity on the formation of precursors, the scattering patterns are compared after 20 min of heating (Figure 4). This plot shows that the formation of the 2.8 nm sized primary units is independent of the alkalinity ($Q \approx 2.2$ nm^{-1}). A maximum in the SAXS pattern is attributed to independent particles with preferred interparticle distances, due to a high concentration and/or due to repulsive interactions. The formation of aggregates (attractive force dominates) results in an increase in intensity at larger *d* spacings compared to the composing particles (smaller *Q* values). For synthesis mixtures having Si/OH ratios of 2.72 and 3.02, we clearly observe the formation of an increased intensity at *Q* values lower than 2.2 nm^{-1}, which corresponds to the formation of aggregates of primary units. At decreasing Si/OH, the scattering at the aggregates decreases, while no indication is observed for a synthesis mixture with Si/OH = 2.12.

The shape of the crystalline product was investigated using transmission electron microscopy. The micrographs of product obtained after 10 h of heating to 125 °C for Si-TPA-MFI synthesis mixtures having various alkalinities show that the

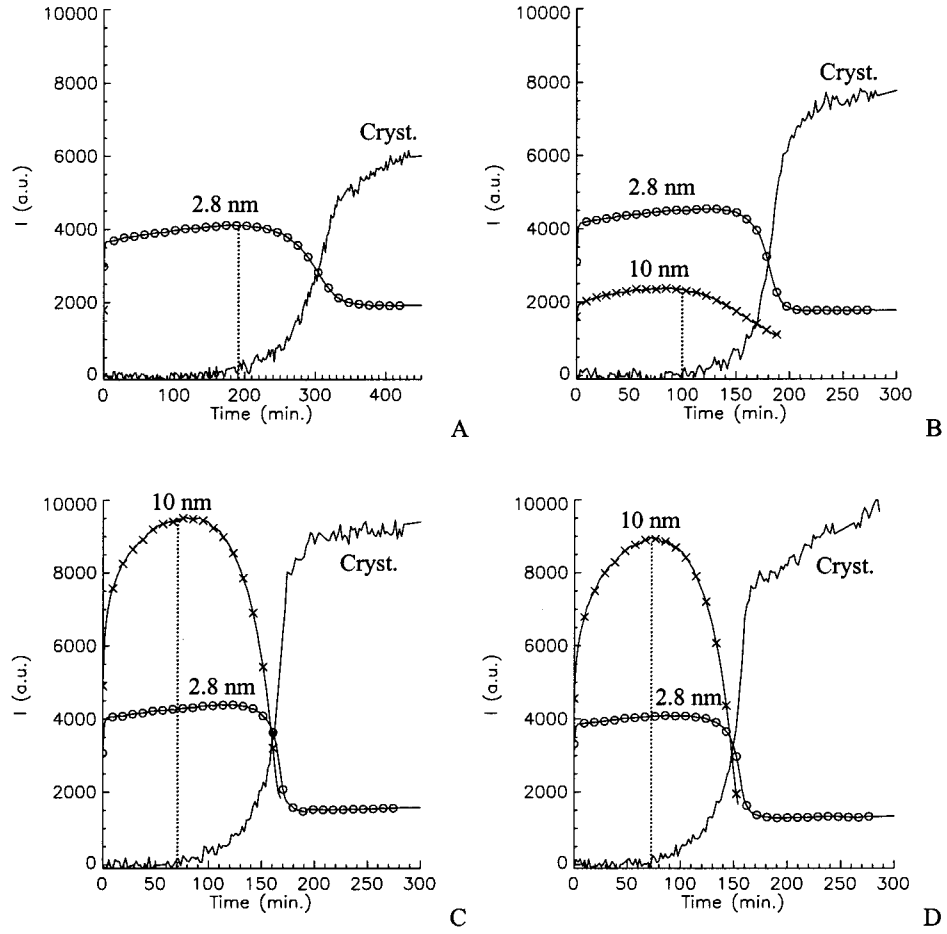

Figure 3. Time-dependent scattering intensity at fixed angles, corresponding with a *d* spacing of 2.8 nm (primary units) and 10 nm (aggregates), together with the area of the Bragg reflections of the product Si-TPA-MFI crystals, for Si-TPA-MFI synthesis mixtures with different Si/OH ratios: (A) 2.42, (B) 2.57, (C) 2.72, (D) 3.02. The scattered intensity at the aggregates (×) has only been plotted when their presence could be demonstrated clearly from the scattering curve, and was divided by 2 for clarity.

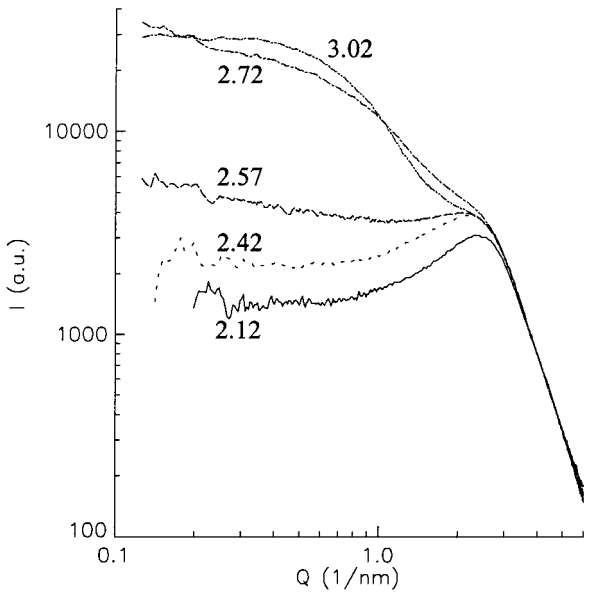

Figure 4. SAXS patterns of Si-TPA-MFI synthesis mixtures after 20 min of heating at 125 °C. Si/OH ratios are denoted at the curves.

product can be classified in two categories depending on the Si/OH ratio of the synthesis mixture (Figure 5). For Si/OH values of 2.72 and 3.02, the crystals are spherical or elliptical and show a cauliflower-like appearance at the surface. For high alkalinities (Si/OH = 2.42 and 2.57), approximately $^2/_3$ of the crystals show multiple intergrowths. The remaining $^1/_3$ of the crystals shows a morphology as found for Si/OH = 2.72 and 3.02. The size of the crystals from the synthesis mixture with Si/OH = 2.42 is larger than the product from solutions with higher Si/OH ratios. TEM micrographs (not shown) from synthesis mixtures with Si/OH = 2.42 which were heated for various times showed that for relatively short reaction times (180 and 250 min) no intergrowths were observed and the crystals had a cauliflower-like appearance. For longer reaction times (400 and 600 min), multiple intergrowths are observed in approximately $^2/_3$ of the crystals.

Crystallization Behavior and Crystal Growth. The rates of conversion of the (amorphous) silica to the crystalline Si-TPA-MFI structure can be determined from the area of the Bragg reflections. In this study, the growth curves of several Bragg reflections have been compared to find whether there was a difference in growth rate in the different crystalline directions, but such a difference has not been found by us for Si-TPA-MFI. The area of the first intense Bragg reflection at $2\Theta = 7.95°$ was used. Figure 6A shows the SiO2 conversion for the synthesis at different alkalinities. This plot shows that the conversion rate does not change very much for Si/OH values of 3.02, 2.72, and 2.57, although a decrease in final peak area can be observed for decreasing Si/OH. There is a significant decrease in conversion rate for higher Si/OH values, and the formation of crystalline material is extremely slow for Si/OH = 2.12 (first sign of Bragg reflection after 25 h of heating, after 60 h intensity ≈10 in same arbitrary units as used in Figure

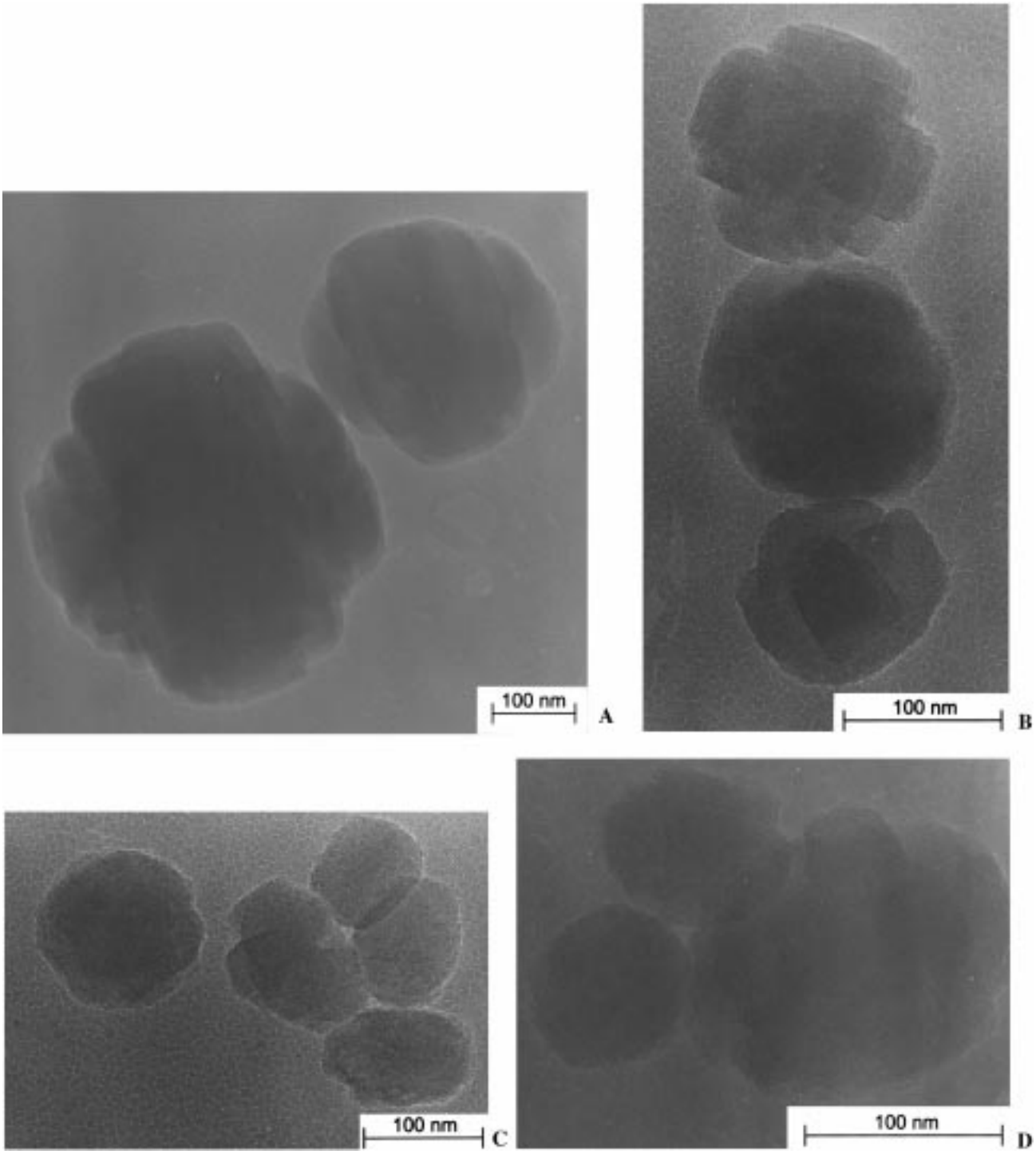

Figure 5. TEM micrographs for Si-TPA-MFI crystals obtained after 10 h of heating to 125 °C for Si/OH ratios of the synthesis mixture of (A) 2.24, (B) 2.57, (C) 2.72, (D) 3.02.

6A). The final area of the Bragg reflections is a measure for the conversion of the SiO2 to zeolite. Figure 6B shows the conversion for synthesis mixtures with different Si/OH ratios as determined in *ex situ* experiments (in stainless steel autoclaves). In order to have a faster conversion to MFI for the synthesis with Si/OH = 2.12, seeds were added, while no seeds were added to the other synthesis mixtures. The addition of a small amount of crystalline SiO2 (<1 wt %) is not expected to influence the final conversion. The same trend for varying alkalinity is oberved both for the final area of the Bragg reflections (Figure 6A) and for the SiO_2 conversion as determined in the ex situ experiments. Note that these values cannot be compared for Si/OH = 2.12 since the area of the Bragg reflection is far from reaching its final value even after 60 h of heating.

From our scattering data we get two types of information about the growing crystals. The Bragg reflections reveal details of the crystal lattice (WAXS or XRD), and the scattering at the surface from the crystals (SAXS) contains information concerning the size and shape of the crystals. Figure 7 compares the area of the Bragg reflections with the scattering intensity at $Q = 0.15\ nm^{-1}$ (d = 42 nm), where the SAXS intensity has been multiplied iwth an arbitrary constant to fit the WAXS curve. For Si/OH = 2.42 (Figure 7A) the same trend is found, but for

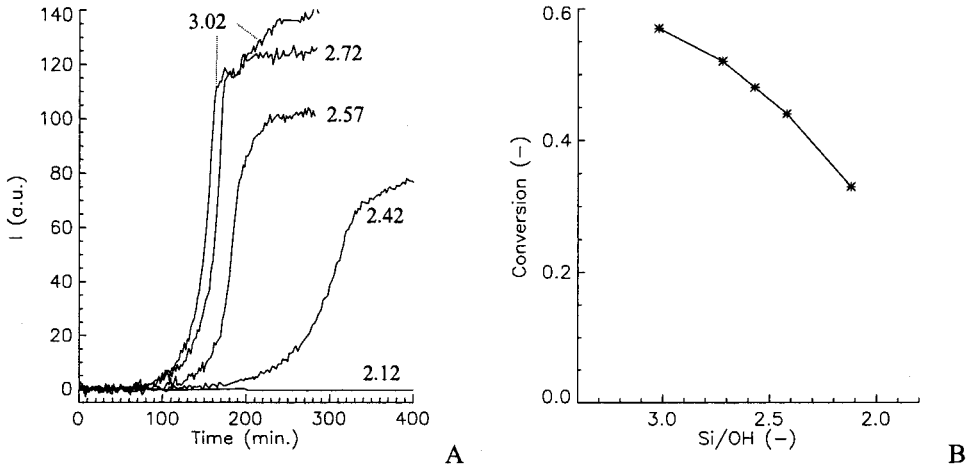

Figure 6. (A) Area of the Si-TPA-MFI Bragg reflections as determined from the WAXS for synthesis mixtures with Si/OH values as denoted at the curves. (B) The conversion of amorphous SiO_2 to Si-MFI for different Si/OH values. Crystallization in stainless steel autoclaves, 24 h at 125 °C. 0.5 wt % seeds have been added in the synthesis with Si/OH = 2.12.

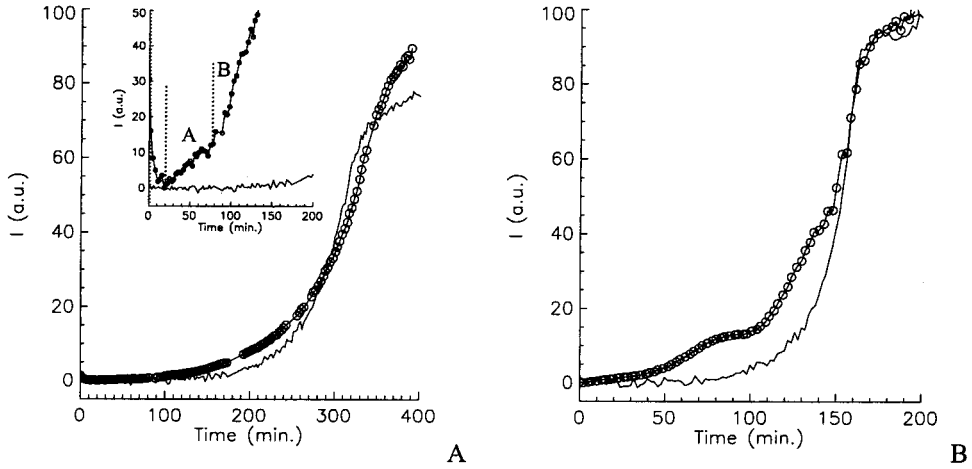

Figure 7. Scattering intensity at the surface of the crystal at $Q = 0.15$ nm-1 (SAXS, ○), and the area of the MFI Bragg reflection (WAXS, solid lines) for Si-TPA-MFI synthesis with Si/OH ratios of (A) 2.42 and (B) 3.02. The intensity of the SAXS has been multiplied with an arbitrary constant. The inset of (A) shows the same plot for short reaction times (different constant in multiplication of SAXS intensity).

Si/OH = 3.02 (Figure 7B) some systematic differences can be observed. As can be seen in Figure 2D, the scattered intensity at $Q = 0.15$ nm^{-1} has a contribution of the scattering at the crystals, as well as from the -10 nm sized aggregates. These results show that one needs to be careful when interpreting the scattering at very low angles as a measure for the crystallinity. For Si/OH = 2.42 the formation of aggregates is not apparent from the scattering curves in Figure 2A. The inset in Figure 7A shows the trends at short reaction times (after 200 min the first sign of Bragg reflections appears). Here the scattering at the surface of the crystal shows two regions: in region A a slow increase in intensity is found, and in region B faster increase is observed. Probably region A is mainly due to scattering at aggregates being formed, and in region B the scattering at the crystals is dominating. Note that this increase in region B is observed well before the formation of Bragg reflections.

To confrim that the growing intensity at the very low Q region is due to scattering at the growing crystals, USAXS experiments have been performed. The Bonse-Hart setup used together with the high-intensity X-rays available at ID2/BL4 of the ESRF allows probing structures with a size up to 6 microns. These results[7] showed that the increase in intensity in the low Q region indeed is due to scattering at the growing crystals. Figure 8 shows the mean size of the crystals as determined by fitting

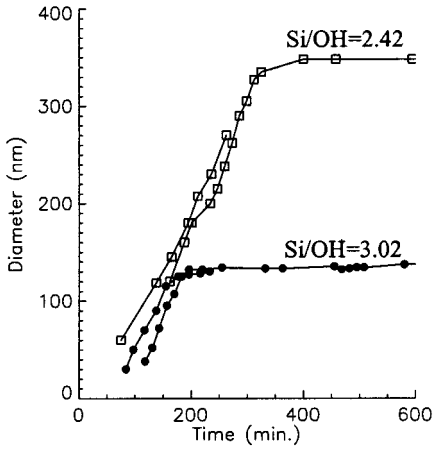

Figure 8. Mean diameter of the crystals as determined by fitting the calculated scattering pattern for a polydisperse system of spheres to the experimental USAXS patterns7 for a synthesis mixtures with Si/OH values of 2.42 (□) and 3.02 (●).

the calculated scattering pattern from a polydisperse system of spheres to experimental USAXS data. The linear growth rate of the crystals was found to e the same for both alkalinities (≈1.2 nm/min), while the final size of the crystals by far was the largest for the synthesis mixture having the highest alkalinity (Si/OH = 2.42).

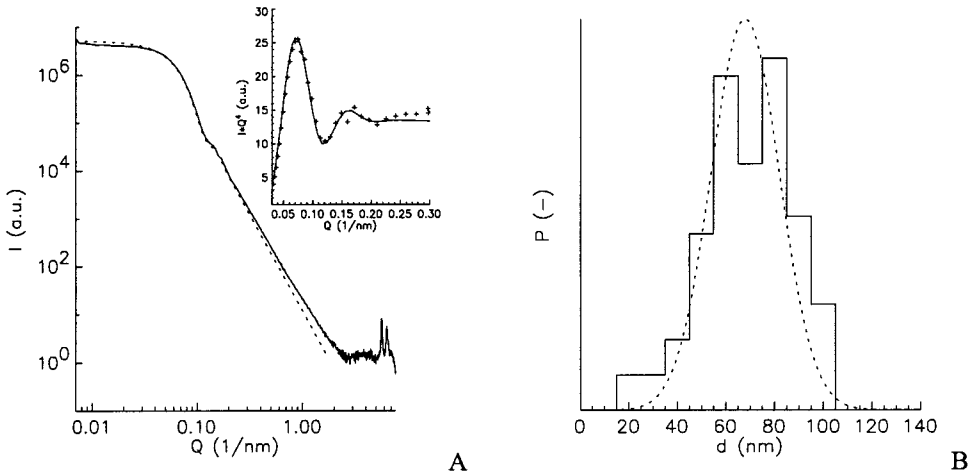

Figure 9. (A) (U)SAXS pattern for the seed suspension (solid line) together with the calculated pattern (dotted line) for apolydisperse system of spheres with a normal distribution having a mean diameter of 68 nm and a standard deviation of 14 nm. The IQ^4 *vs* Q plot in the inset clearly shows the form factor oscillations in both experimental (+) and calculated data (solid line). (B) The particle size distribution used for the calculation (dotted line) and the size distribution of the seed crystals as determined from EM images (88 crystals measured).

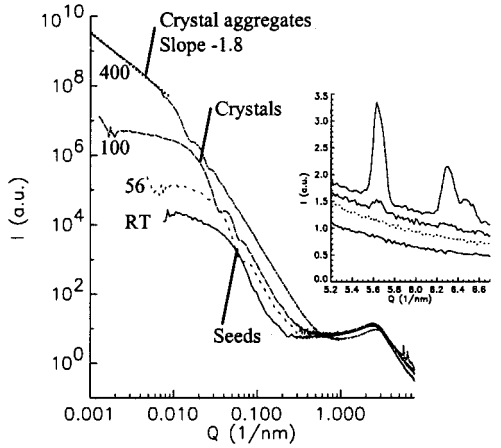

Figure 10. Si-TPA-MFI crystallization from a synthesis mixture with Si/OH = 2.12 having 0.1 wt % seeds. The reaction times at 125 °C are denoted at the curves. The inset focuses on the formation of the Bragg reflections in the high-Q region.

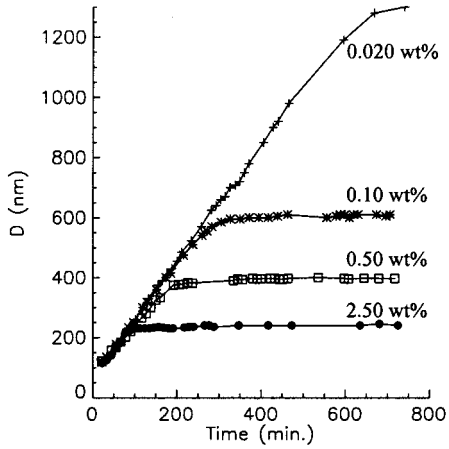

Figure 11. Mean crystal diameter as determined from fitting the calculated scattering pattern of a polydisperse system of spheres to the experimental USAXS patterns for a synthesis mixture with Si/OH = 2.12 with seeds added. The weight percentage seeds (g of SiO_2 seeds g of SiO_2 in synthesis mixture) is denoted at the curves.

Influence of Seeds. Figure 6 shows that the conversion of silica to MFI is extremely slow for the synthesis mixture having Si/OH = 2.12. To be able to discern whether this slow crystallization is due to difficult nucleation or to crystal growth (or both), reactions were performed with addition of various amounts of SI-TPA-MFI seeds to the fresh synthesis mixture. To identify the seeds, the stable colloidal seed suspension was investigated with X-ray scattering and EM. Figure 9A shows the scattering pattern of a seed suspensions (2.684 wt % SiO2) compared with the calculated scattering pattern for a polydisperse system of spheres with a normal distribution with a mean diameter of 68 nm and a standard deviation of 14 nm. This particle size distribution shows good agreement with that as determined from EM images (Figure 9B).

Various amounts of seeds were added to fresh synthesis mixtures with Si/OH = 2.12 and in all cases a high increase in the crystallization rate was observed compared to the unseeded synthesis mixture. Figure 10 shows the scattering patterns for the synthesis mixture with 0.1 wt % seeds. The scattering pattern after addition of the seed crystals at room temperature (Figure 10, RT), confirms that the scattering at crystals is detected earlier from the scattering at the surface of the crystals in the SAXS regime compared to the diffraction from the internal crystal lattice in the WAXS regime (as illustrated also in Figure 7A). After heating, the growth of the crystals can be followed in the USAXS regione due to scattering at their surface. When the growth of the crystals has finished, a sudden aggregation of the crystals is observed to aggregates with a size larger than 6 mm (Figure 10, 400 min). The actual size of the aggregates cannot be determined since their size exceeds the maximum d spacing probed in the USAXS experiments. The slope of the linear region in the log I *vs* log Q plot due to the scattering at these aggregates is −1.8, which is in agreement with the scattering at aggregates formed by a diffusion-limited aggregation process.

The size distribution of the growing seed crystals was estimated by fitting the calculated scattering pattern of a polydisperse system of spheres to the measured USAXS pattern for synthesis mixtures having Si/OH = 2.12 with 2.5, 0.5, 0.1, and 0.02 wt % seeds added. The evolution of the mean crystal diameter during synthesis for all systems is shown in Figure 11. As expected, a synthesis mixture without seeds showed no scattering intensity above the background pattern until the experiment was stopped after 11 h of heating (because of end of beamtime at the ESRF). For all seed concentrations, a linear growth is observed, after which the size of the crystals is constant. The linear growth rate is approximately 1.8 nm/min independent of the seed concentration (Table 1). Surprisingly,

TABLE 1: Crystallization Si-TPA-MFI from Synthesis Mixture with Si/OH = 2.12 with Various Amounts of Seeds[a]

wt % seeds	end linear growth (min)	final size (nm)	conversion (SiO_2 basis)	offset (nm)	growth rate (nm/min)	fraction growing seeds
2.50	90	240	0.34	64	1.8	0.34
0.50	190	397	0.32	68	1.6	0.36
0.10	295	610	0.32	68	1.8	0.49
0.02	≈650	≈1300	0.31	65	1.9	0.25

[a] The offset and growth rate are calculated from the linear fit to the data in the linear growth region. The offset is the extrapolation to zero reaction time.

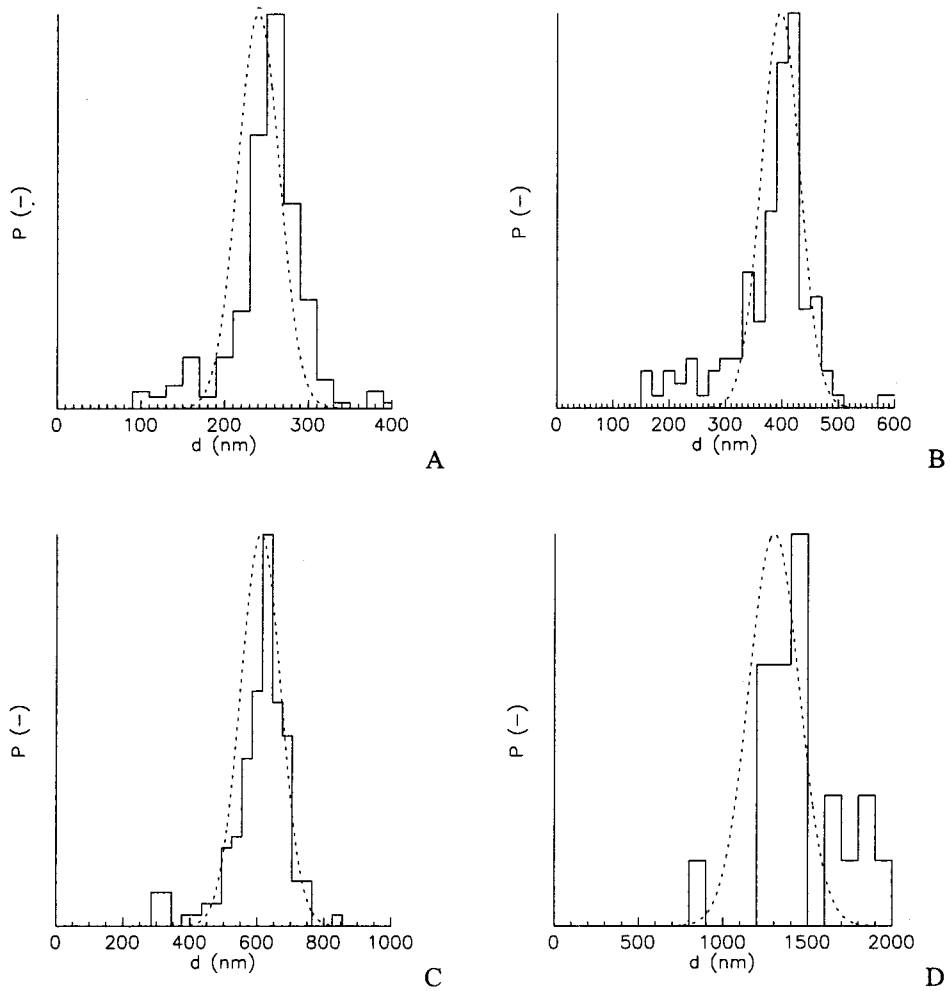

Figure 12. Crystal size distribution for Si-TPA-MFI synthesis mixtures with Si/OH = 2.12 and various amounts of seed crystals after 12 h of heating at 125 °C. The dotted line gives the size distribution as resulted from the fitting procedure of the USAXS data. The histogram is the result of measured particle sizes from EM images. (A), (B), (C), and (D) represent 2.50, 0.50, 0.10, 0.020 wt % seeds, respectively, and the number of crystals measured from EM images is 228, 142, 144, and 21, respectively.

this growth rate is not the same as for unseeded synthesis mixtures having Si/OH = 2.42 and 3.02 (Figure 8), but approximately 50% higher. A similar increase in growth rate for seeded versus unseeded synthesis mixtures has been observed before by Twomey *et al.*[23] The size of the extrapolation of the linear growth curve to zero reaction time shows an initial mean crystal diameter which is in good agreement with the mean size of the seeds. The final size of the crystals increases with the decreasing amount of seeds, which can be explained by an increasing amount of nutrients available per growing crystal. The SiO_2 conversion after 12 h of heating was determined from *ex situ* experiments in stainless steel autoclaves. The fraction amorphous SiO_2 converted into MFI was fairly constant at 0.32 for all amounts of seeds added (see Table 1). For the case with 0.020 wt % seeds, the end of the linear growth region and the final crystal size cannot be determined accurately since the growth curve just levels off near the end of the experiment (Figure 11, around 650 min). However, according to the SiO_2 conversion the reaction is expected to be finished after 12 h of heating, since then the SiO_2 conversion was found to be independent of the amount of seeds (Table 1).

The comparison of the particle size distributions as determined by the fitting procedure with USAXS patterns and from electron microscopy images (Figure 12) reveals some small systematic differences between the results of the two methods. The maximum in the particle size distribution is at slightly larger diameters for the EM results compared to the fitting results. Also, the particle size distribution from the EM results appears not to be symmetric, having a longer tail on the small diameter side of the maximum (except for 0.020 wt % seeds, but the histogram from the EM results is based on a small number of crystals and therefore not very reliable). Altogether there is satisfying agreement between the results of the two methods.

The number of crystals in the product relative to the number

of seeds added can be calculated using the particle size distribution of both seeds and product, the weight fraction seeds added, and the SiO_2 conversion. Here the particle size distribution as resulted from the fitting procedure has been used to calculate the average volume of the seeds and the crystals in the final product. This ratio does not show a clear trend with the weight fraction of seeds, but the results show that the number of crystals in the final product is about $^1/_3$ of the number of seeds added. The electron microscopy images of the product did not show the presence of unreacted seed crystals (Figure 12).

Synthesis Temperature. To determine the activation energy for crystal growth, the crystallization from synthesis mixtures with Si/OH = 2.42 was performed at various temperatures, and was studied *in situ* with USAXS. The mean diameter of the growing crystals was determined by fitting the calculated scattering pattern of a polydisperse population of spherical crystals to the measured USAXS curve. Figure 13A shows the size evolution of the crystals as a function of reaction time. From this plot it is clear that the crystals grow linearly in time and that the expected lower linear growth rate is found for lower reaction temperatures. For reaction temperatures of respectively 110, 125, 140, and 160 °C, the linear growth rate was respectively 0.36, 1.35, 3.49, and 10.4 nm/min. The particle size distributions of the final product for the syntheses at 140 and 160 °C as determined from the USAXS fitting procedure and from EM images show good agreement (Figure 13A, inset). The apparent activation energy for Si-TPA-MFI crystal growth was determined to be 83 kJ/mol from the Arrhenius type of plot in Figure 13B. In the literature there is quite some scattering in the value for the apparent activation for crystal growth (Table 2).

Discussion

Precursor and Product Particles. The small-angle scattering patterns (Figures 1 and 2) provide information on the formation and consumption of nanometer scale precursor particles and the crystalline product. Irrespective of the alkalinity, the presence of 2.8 nm sized primary units was observed from the onset of the reaction. The primary units are therefore expected to be formed during the dissolution of the silicic acid in the TPAOH solution. The estimated size of these particles is the same as reported for visible light scattering experiments by Schoeman.[13,14] From NMR experiments, it is know that silicate species interact with TPA cations before the onset of crystallization.[5] TPA is clearly identified as being present in the precursor particles from contrast variation SANS experiments on synthesis mixtures[15] and Raman experiments on particles extracted from the aqueous solution.[13] Ordering in the silica (observation of 560 cm^{-1} IR band) in structures typical for the MFI crystal topology was observed before the onset of the crystallization.[6] Combining this evidence from varying experiments, we believe the observed particles to be composite organic−inorganic particles which do contain some ordering of the silica related with the MFI structure, but not fully organized yet in a crystalline lattice.

The formation of a second population of precursor particles is observed to be strongly dependent on the alkalinity of the synthesis mixture (Figure 4). These particles are believed to be aggregates of the primary units, and the scattering curves (Figure 2C,D) show that their size increases with reaction time to approximately 10 nm until they are consumed in the crystallization process.

From our X-ray scattering data on crystallizations from clear solutions, there are two methods to track the formation of

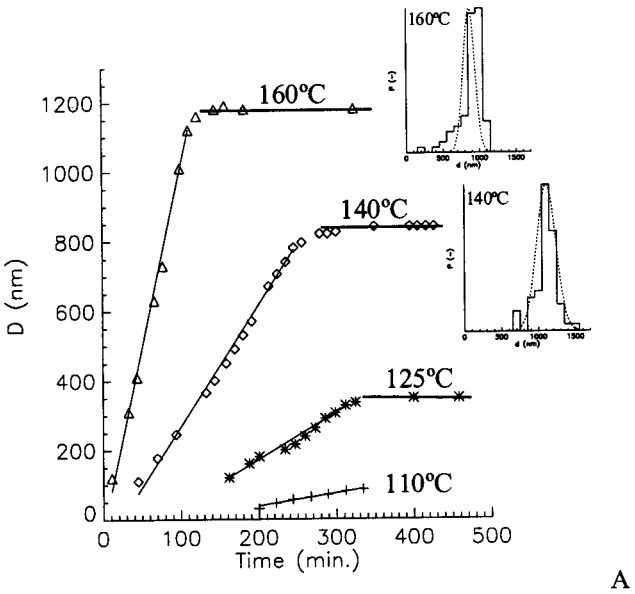

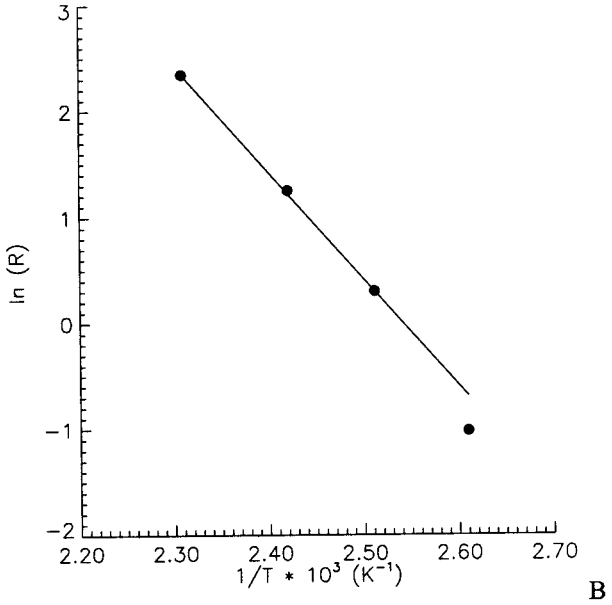

Figure 13. (A) Crystal growth for synthesis mixtures with Si/OH = 2.42 at various temperatures as denoted at the curves. The insets show the particle size distribution of the final product as determined from the fitting procedure and from EM images for reaction temperatures of 140 and 160 °C. (B) Arrhenius plot from the linear growth rates of the diameter of the crystals as determined from the growth curves.

crystals (third particle population): from the scattering at the crystal surface, which is observed at relatively large length scales (small angles), and from the diffraction at the internal crystalline lattice of the crystals (Bragg reflections). Figure 7A illustrates that the scattered intensity at the surface of the crystal is observed much earlier than the diffraction at the crystalline lattice (also clear in Figures 1, 2, and 10 (RT)). However, one has to be careful in the interpretation of the scattering intensity at very low angles, since also the scattering at large, noncrystalline structures as the aggregates of primary units is observed in this region (Figure 7B). Therefore, the area of the Bragg reflections as observed in the high-Q region is taken as a measure for the conversion of SiO_2 to crystalline material.

Role of Nanometer Scale Precursors. To elucidate the role of the precursor particles, their formation and consumption has to be related to the crystallization behavior. Figure 6B shows that the final SiO_2 conversion decreases with increasing alkalin-

TABLE 2: Apparent Activation Energy for Si-TPA-MFI Crystal Growth in the Length and the Width ($E_{lengths}$ and E_{width}), and for Crystals ($E_{crystal}$) When No Distinction was Made[a]

source	E_{length} (kJ/mol)	E_{width} (kJ/mol)	$E_{crystal}$ (kJ/mol)
Schoeman et al.[19]			42
Sano et al.[20]	61	36	(48)
Feoktistova et al.[21]	64.5	46.5	(55)
Cundy et al.[22]	79	62	(70)
Watson et al.[15]			70
this study			83
Twomey et al.[23]			96

[a] The values in parentheses for crystal growth were calculated here from the reported values for length and width growth by averaging, for comparison of the activation energies for crystal growth.

ity. This can be explained by a higher dissolution rate of the crystals at higher alkalinity. For Si/OH ratios of 3.02, 2.72, and 2.57 the rate of SiO_2 conversion to MFI is similar, as is shown in Figure 6A. For lower Si/OH values (higher alkalinities) however, a clear decrease in conversion rate is observed, whereas the rate is extremely slow for Si/OH = 2.12. Also, the fitting of the USAXS patterns shows that the growth rate of the crystals is the same for Si/OH = 2.42 and 3.02. This means that the slower conversion of SiO_2 to Si-MFI for increasing alkalinity cannot be attributed to a lower growth rate (higher dissolution rate) of the crystals, but results from a lower number of crystals due to a reduced rate of nucleation.

This is affirmed by the experiments with Si/OH = 2.12, which shows a very slow crystallization (Figure 6A). This would mean that growth does not occur since the crystallization is blocked due to the absence of nucleation. As a control experiment to check whether a synthesis mixture is able to grow Si-TPA-MFI crystals, seeds were added to bypass the nucleation step. The scattering experiments (Figure 10) show that normal crystal growth is observed when seeds have been added to a fresh synthesis mixture having a Si/OH ratio of 2.12. This proves that in a synthesis mixture having Si/OH = 2.12 without seeds, nucleation is (almost) impossible, while growth is possible once crystals are present.

By simultaneously measuring small- and wide-angle scattering, we are able to correlate the crystallization behavior to the presence and consumption of nanometer scaled precursor particles. Figure 4 illustrates that the 2.8 nm sized primary units are an invariant for Si-TPA-MFI synthesis mixtures with varying alkalinity. On the contrary, the formatio of aggregates of these primary units is dependent on the alkalinity and shows a strong correlation with the number of crystals, i.e., the rate of nucleation: a hish nucleation rate is observed when a high concentration of aggregates is observed (high Si/OH ratios), while the nucleation rate (almost) vanishes when no formation of aggregates is observed. The formation of aggregates of primary units is therefore believed to be an essential step in the nucleation.

The role of the primary units and their aggregates is confirmed by the evolution of their concentrations in relation to the conversion of amorphous SiO_2 to Si-MFI. The role of the aggregates in the nucleation process is strengthened by the onset of their consumption at the onset of the crystallization (FIgure 3B,C,D). The strong decrease of the scattered intensity from the aggregates also shows that only a small fraction of them transforms in viable nuclei, and that the vast majority dissolves to smaller precursor particles. The scattering at the primary units is almost constant until most of the aggregates have disappeared as shown in Figure 3 and Figure 2B,C,D (third curve). Probably the dissolution of the aggregates compensates the consumption of the primary units in the crystallization process. After the aggregates have disappeared, a fast consumption of the primary units is observed. Therefore, the omnipresent 2.8 nm sized primary units probably play a key role in the crystal growth process.

Seeding. The influence of seeding on the crystal growth behavior was investigated for Si-TPA-MFI synthesis mixtures with Si/OH = 2.12, showing very slow nucleation when no seeds are added. The crystal growth history was followed by fitting the scattering pattern of a polydisperse system of interacting spheres with the experimental scattering patterns. Also, the size distributions from the fitting procedure at the scattering curves of the seed crystals (Figure 9) and final product of the reactions (Figure 12) show good agreement with those as determined from the EM images. Therefore, we believe that the fitting procedure of the scattering data yields reliable information on the size history of the crystals. An advantage of using small-angle X-ray scattering for this purpose is that this allows to determine *in situ* the crystal growth over the whole length range on one sample, even when the system is gets turbid during the synthesis.

Figure 10 illustrates that the scattering patterns for a synthesis mixture having Si/OH = 2.12 with 0.10 wt % seeds added show strong agreement with the patterns for a synthesis mixture having Si/OH = 2.42 without seeds (Figure 2A). When the growth of the crystals has finished, the discrete crystals are observed to aggregate with a mass fractal dimension of 1.8 (Figure 10, 400 min). This feature was previously observed for unseeded synthesis mixture having Si/OH = 2.42 and 3.02 (ref 7). The size of the aggregates could not be determined, since it exceeds the maximum probed length scale of 6 microns. This sudden aggregation of the discrete crystals is believed to be due to a change in the composition of the solution, resulting in a decrease of the repulsive forces between the crystals.

The number of crystals in the product relative to the number of seeds added can be calculated from the silica conversion, the weight fraction of seeds added, and the particle size distributions of the seed crystals and the final product. This fraction shows that the number of crystals in the final product is in the order of one-thrid of the number of seeds (Table 1). A possible effect is that the seeds added do not grow but that they only induce nucleation in synthesis mixtures that show no nucleation in the unseeded situation. But, the offset of the growing crystals for the synthesis mixtures having various degrees of seeding in all cases is close to the size of the seed crystals. Therefore, it is believed that it is the actual seeds added that grow to the final product crystals. Another possible explanation of the fact that just one-third of the seeds grows to crystals is that a fraction of them is inert. This is not believed to be the case since no crystals in the size range of the seeds are observed in the electron microscopy images of the product. Therefore, we believe that approximately one-third of the seeds added to the synthesis mixture grows, while the rest (predominantly the smaller fraction) dissolves, similar to Ostwald ripening in silica particles.[16]

By varying the amount of seed crystals, we are able to control the number of growing crystals in the synthesis mixture. Figure 11 shows that the linear growth rate is independent of the weight fraction of seeds (ranging from 0.020 to 2.5 wt %). Therefore, the formation of structures which are consumed in the crystal growth process is not the rate-limiting steps. This is in agreement with the observation that the 2.8 nm sized primary units are present from the start of the reaction. The growth rate

dependence on the reaction temperature shows an apparent activation energy for crystal growth of 83 kJ/mol (Figure 13). Although there is significant scattering in this value in literature, all values are well above the activation energy of 12−17 kJ/mol which is to be expected for a diffusion-controlled growth mechanism.[17] In a previous study,[18] we found the conversion of SiO_2 to MFI to be independent of the concentration of the synthesis mixture, which also means that the crystal growth is not diffusion controlled. This is in accord with the abundant presence of the primary units and with a growth mechanism where the integration of the primary units at the crystal surface is the rate-limiting step.

Conclusions

The results presented here show that a combination of USAXS and SAXS/WAXS experiments is a powerful tool to probe *in situ* a broad range of length scales covering all precursor and product particle populations during the whole course of the zeolite crystallization. The crystal particle size distribution as determined from the fitting of a calculated scattering pattern of a polydisperse system of spheres to the measured patterns shows good agreement with the distribution as determined from electron microscopy images.

For the crystallization of Si-TPA-MFI from a clear synthesis mixture, three particle populations are observed: primary units and their aggregates are precursors which are consumed during the formation of the product, the crystals. By varying the alkalinity of the fresh synthesis mixtures and the use of seed crystals we were able to show that the aggregation of the 2.8 nm sized primary units is an essential step in the nucleation process. The crystal growth probably is the reaction-controlled integration of primary units at the crystal surface.

Acknowledgment. Ernie Komanschek is acknowledged for his help at and around the Daresbury synchrotron. The SAXS/WAXS experiments were performed at the Daresbury Synchrotron Radiation Source by an EPSRC grant. We thank Olivier Diat for setting up and aligning the Bonse-Hart setup. USAXS experiments were performed at the European Synchrotron Radiation Facility at ID2/BL4. Patricia Kooyman of the National Centre for High Resolution Electron Microscopy, Delft University of Technology, Delft, The Netherlands, is acknowledged for performing the electron microscopy investigations. We thank Exxon Chemical and Mark Davis for the fruitful discussions.

References and Notes

(1) Van Bekkum, H., Flanigen, E. M., Jansen, J. C., Eds. *Introduction to zeolite science and practice*; Stud. Surf. Sci. Catal. Elsevier: New York, 1991; Vol. 58.

(2) Davis, M. E.; Katz, A.; Ahmad, W. R. Chem. Mater. **1996**, *8*, 1820−1839.

(3) Davis, M. E.; Lobo, R. F. *Chem. Mater.* **1992**, *4*, 756−768.

(4) Bell, A. T. In *Zeolite synthesis*; Occelli, M. L., Robson, H. E., Eds.: ACS Symp. Ser. 398; American Chemical Society: Washington DC, 1989; pp 66−82.

(5) Burkett, S. L.; Davis, M. E. *J. Phys. Chem.* **1994**, *98*, 4647−4653.

(6) Burkett, S. L.; Davis, M. E. *Chem. Mater.* **1995**, *7*, 920−928.

(7) De Moor, P.-P.E.A.; Beelen, T. P. M.; Komanschek, B. U.; Diat, O.; Van Santen, R. A. *J. Phys. Chem. B* **1997**, *101*, 11077−11086.

(8) Verduijn, J. P. Exxon patent, PCT/EP92/02386, 1992.

(9) Bras, W.; Derbyshire, G. E.; Ryan, A. J.; Mant, G. R.; Felton, A.; Lewis, R. A.; Hall, C. J.; Greaves, G. N. *Nucl. Instrum. Methods Phys. Res. Sect. A* **1993**, *326*, 587.

(10) Diat, O.; Bosecke, P.; Lambard, J.; De Moor, P.-P.E.A. *J. Appl. Cryst.* **1997**, *30*, 862.

(11) Mulato, M.; Chambouleyron, I. *J. Appl. Cryst.* **1996**, *29*, 29−36.

(12) Pedersen, J. S. *J. Appl. Cryst.* **1994**, *27*, 595−608.

(13) Schoeman, B. J. In *Progress in zeolite and microporous materials*; Chon, H., Ihm, S.-K., Uh, Y. S., Eds.; Stud. Surf. Sci. Catal.; Elsevier Science B.V.; Amsterdam, 1997; Vol. 105, pp 647−654.

(14) Schoeman, B. J. *Zeolites* **1997**, *18*, 97−105.

(15) Watson, J. N.; Iton, L. E.; Keir, R. I.; Thomas, J. C.; Dowling, T. L.; White, J. W. *J. Phys. Chem. B* **1997**, *101*, 10094−10104.

(16) Iler, R. K. *The chemistry of silica*; John Wiley & Sons: New York, 1979.

(17) R. M. Barrer, *Hydrothermal Chemistry of Zeolites*; Academic Press: London, 1982, Chapter 5.

(18) De Moor, P.-P.E.A.; Beelen, T. P. M.; Van Santen, R. A. *J. Appl. Cryst.* **1997**, *30*, 675−679.

(19) Schoeman, B. J.; Sterte, J.; Otterstedt, J. E. *Zeolites* **1994**, *14*, 568−575.

(20) Sano, T.; Sugawara, S.; Kawakami, Y.; Iwasaki, A.; Hirata, M.; Kudo, I.; Ito, M.; Watanabe, M. In *Zeolites and Related Microporous Materials: State of the Art 1994*; Stud. Surf. Sci. Catal. Elsevier Science: New York, 1994; Vol. 86, pp 187−194.

(21) Feoktistova, N. N.; Zhdanov, S. P.; Lutz, W.; Bulow, M. *Zeolites* **1989**, *9*, 136−139.

(22) Cundy, C. S.; Lowe, B. M.; Sinclair, D. M. *Faraday Discuss.* **1993**, *95*, 235−252.

(23) Twomey, T. A. M.; Mackay, M.; Kuipers, H. P. C. E.; Thompson, R. W. *Zeolites* **1994**, *14*, 162−168.